ELSEVIER

Journal of Nuclear Materials 307–311 (2002) 484–489

journal of nuclear materials

www.elsevier.com/locate/jnucmat

Tensile and fracture toughness properties of MA957: implications to the development of nanocomposited ferritic alloys

M.J. Alinger *, G.R. Odette, G.E. Lucas

Department of Materials, University of California, Santa Barbara, CA 93106, USA

Abstract

A study to explore approaches to optimizing nanocomposited ferritic alloys was carried out on dispersion strengthened mechanically alloyed (MA) MA957, in the form of extruded bar stock. Previous studies had indicated that this alloy manifested superior high temperature strength and radiation stability, but was extremely brittle in notch impact tests. Thus our objective was to develop a combination of tensile, fracture toughness and microstructural data to clarify the basis for this brittle behavior. To this end, tensile properties and fracture toughness were characterized as a function of temperature in various orientations relative to the grain and inclusion structures. This database along with extensive fractography suggests that brittleness is due to the presence of a large volume fraction of impurity alumina stringers. In orientations where the effects of the stringers are reduced, much higher toughness was observed. These results provide a path for alloy development approach to achieve high strength and toughness.

1. Introduction

Iron based alloys, strengthened with a high number density of ultra-fine, nanometer-scale yttria–titanium–oxygen complex particles have demonstrated outstanding high temperature creep strength. This high strength, coupled with chromium additions for corrosion resistance, offers great promise for elevated temperature applications in fusion first wall and blanket structures [1]. However, an intrinsic challenge in the development of these alloys is maintaining adequate fracture toughness in combination with high creep strength. Mechanical alloying (MA) ferritic powders with Y_2O_3 and Ti by high-energy mechanical milling, followed by consolidation at elevated temperature produces ultra-fine, nm-scale, coherent Y–O–Ti clusters, as well as a more typical fine-to-coarser scale incoherent $Y(Ti)_2O_3$ dispersed oxide particles [1]. These alloys are typically referred to as oxide dispersion strengthened steels. Given their engineered microstructural architectures and extremely low carbon content, which we believe will be a key factor in their success, a more applicable nomenclature for this class of materials is nanocomposited ferritic alloys (NFAs).

There are various approaches to optimizing the microstructures of NFAs. A common set of desirable features include: (a) an as fabricated ferritic matrix structure with the grains, dislocations and precipitate phases balanced to resist swelling and remain stable; (b) a high density of thermally and irradiation stable nano-dispersiods to provide both high creep and tensile strength and to act as helium trapping sites; (c) minimal impurity, inclusion and brittle second phase contents; and (d) low porosity following consolidation. The grain structure is very important and must be optimized. Since

* Corresponding author. Tel.: +1-805 893 3212; fax: +1-805 893 8651.

E-mail address: alinger@engineering.ucsb.edu (M.J. Alinger).

0022-3115/02/$ - see front matter
PII: S0022-3115(02)01220-5

recrystallization temperatures are very high, fine grain structures are generally expected. The effect of grain structures on diffusion creep (possibly detrimental) and fracture (possibly beneficial) depends on the balance of the alloy microstructure and must be better understood. The grain structures are also highly anisotropic and textured following typical extrusion processing steps. While such structures are generally viewed as undesirable, their actual effects on properties depend on the particular situation and are not yet well understood.

We are in the process of fabricating small batches of NFAs for both fundamental studies of nano-microstructural control and stability as well as for establishing structure-property relations. However, in this paper we focus on the characterization of the fracture toughness and tensile properties of a patented (US Patent 4 075 010) commercially produced NFA, MA957 [2]. Low toughness is a potential problem with NFAs since, in common with other BCC metals and alloys, they exhibit a ductile to brittle fracture mode transition over a characteristic range of temperature. Further, the very high strength of NFAs would be expected to result in decreased toughness relative to that of conventional steels. As noted above, during extrusion processing, MA957 (and similar alloys) develop highly anisotropic grain structures resulting in variations in properties with specimen orientation. Moreover, MA processing routes are vulnerable to impurity contamination. The MA957 product examined here was contaminated by a substantial volume fraction of alumina (Al_2O_3) stringers from impurities in the ferrochrome powder source of the master alloy [3].

2. Experiment

The MA957 was provided by Gelles of PNNL in the form of a hot-extruded bar produced by International Nickel Company (INCO) [4]. The nominal chemical composition is 14Cr–0.9Ti–0.3Mo–0.25Y_2O_3. Details of the processing can be found in Ref. [3]. Previous microstructure characterization showed highly anisotropic structures with equiaxed grains in the transverse direction (≈0.5 μm) but with significant elongation in the longitudinal direction resulting in a ≈10:1 grain aspect ratio. Alumina stringers aligned in the longitudinal direction were also observed [3].

Small, 1/3 Charpy-sized three-point bend specimens ($3.33 \times 3.33 \times 18$ mm^3) were electro-discharge machined from the as-received bar in three orientations with respect to the extrusion direction (see Fig. 1). Per ASTM Standard E399, these orientations included: (a) circumferential-transverse/length-longitudinal crack plane (C–L); (b) circumferential-transverse/length-radial crack plane (C–R); and (c) longitudinal/length-radial crack plane (L–R) [5]. The specimens were pre-cracked from a starter notch length (a) to width (W) ratio of 0.5 and tested quasi-statically in three-point bending over a range of temperatures encompassing the key fracture mode and toughness transitions. At low temperatures fracture was linear elastic and K_{Ic} was analyzed in accordance with ASTM E399. At higher temperatures in the transition, fracture was by elastic-plastic cleavage and the toughness K_{Jc} or K_q was evaluated following the general procedures in ASTM E1921-97 [6]. The K_q indicates that the deformation at fracture was sufficient to

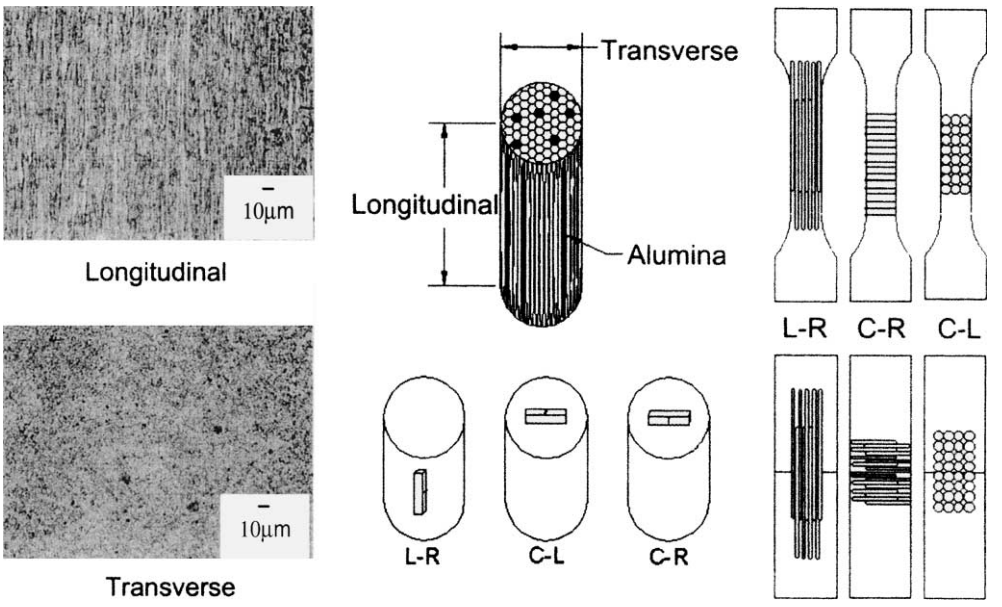

Fig. 1. Three-point-bend and tensile specimen orientation showing grain anisotropy and alumina (Al_2O_3) stringers.

indicate potential for significant constraint loss or ductile tearing before cleavage. At still higher temperatures the sharp pre-cracks grew by ductile tearing type processes. There was no attempt to measure J_R–da curves in this case, and effective tearing toughness was determined based on an elastic-plastic maximum load criteria, K_m.

The tensile testing was conducted with small flat tensile specimens (0.5 mm thick, 9 mm gauge length) that were electro-discharge machined from the as-received bar in the three orientations that, shown in Fig. 1, are designated as being perpendicular to the crack plane of the fracture specimens. These specimens were tested at a strain rate of 1.33×10^{-3} s^{-1} in accordance with testing guidelines in ASTM E8 [7].

3. Results and analysis

3.1. Three-point bend

Figs. 2–4 summarize the toughness versus temperature data for the specimens tested in the three orientations. The filled triangles, circles and diamonds respectively indicate: (a) linear elastic cleavage fracture (K_{Ic}); (b) elastic-plastic cleavage, including cases where some stable crack growth was mixed with pop-ins (K_{Jc} or K_q); and (c) stable crack growth by ductile tearing with minimal pop-ins (K_m). A representative micrograph of the fracture surface in the various fracture regimes, an orientation diagram and the trend lines for the other two orientations are also shown. The white arrows on the micrographs indicate the macroscopic crack propagation direction. It is evident that the toughness, the cleavage transition temperature regime, as well as the basic fracture process itself, are highly dependent on orientation as mediated by the grain and inclusion substructure.

The results for the L–R orientation shown in Fig. 2 exhibit the highest toughness and the lowest cleavage transition temperature. The transition to stable crack growth occurs at about −70 °C. However, even at much lower temperatures, down to about −145 °C, fracture occurs by a series of *small* pop-in events with what appears to be some of intervening stable growth. The micrographs show cracking in the L–R orientation is primarily out-of-plane, transverse to the fracture surface, which manifests substantial levels of plastic deformation.

The toughness levels for both circumferential orientations are much lower. Fig. 3 shows the results for the C–R orientation, with intermediate toughness. Below about 50 °C fracture is linear elastic ranging from K_{Ic} 25–60 MPa $\sqrt{m}$. Between 70 and 100 °C there is some plasticity prior to cleavage, but the toughness remains low, with $K_{Jc} \leqslant 75$ MPa $\sqrt{m}$. Ductile tearing occurs above about 100 °C at a *very* low value of 75 MPa $\sqrt{m}$. The micrographs show that the fracture path in the C–R orientation also has somewhat torturous out-of-plane components with ductile dimples mixed with cleavage facets on the fracture surface.

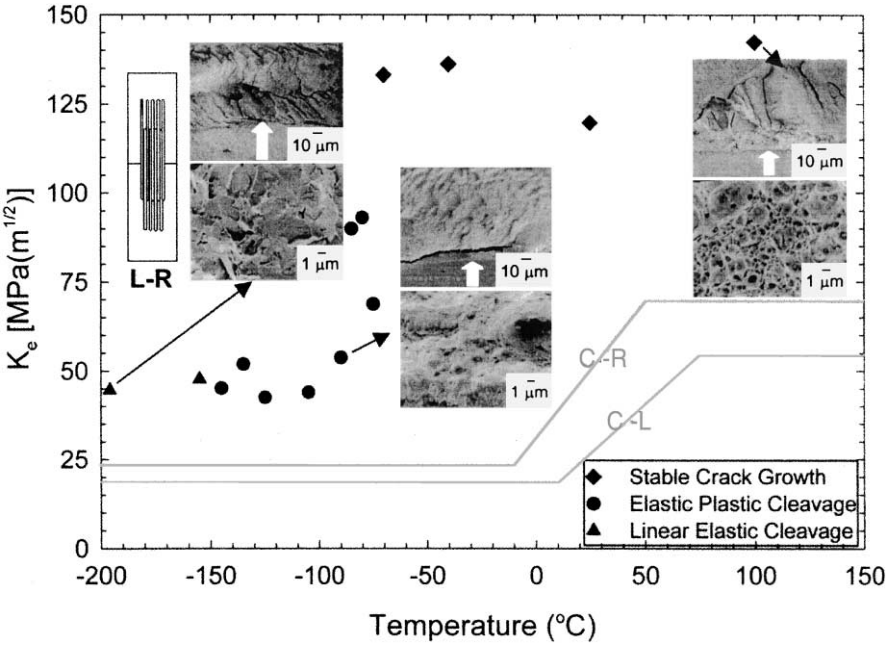

Fig. 2. K_e vs. test temperature and corresponding micrographs for the L–R orientation.

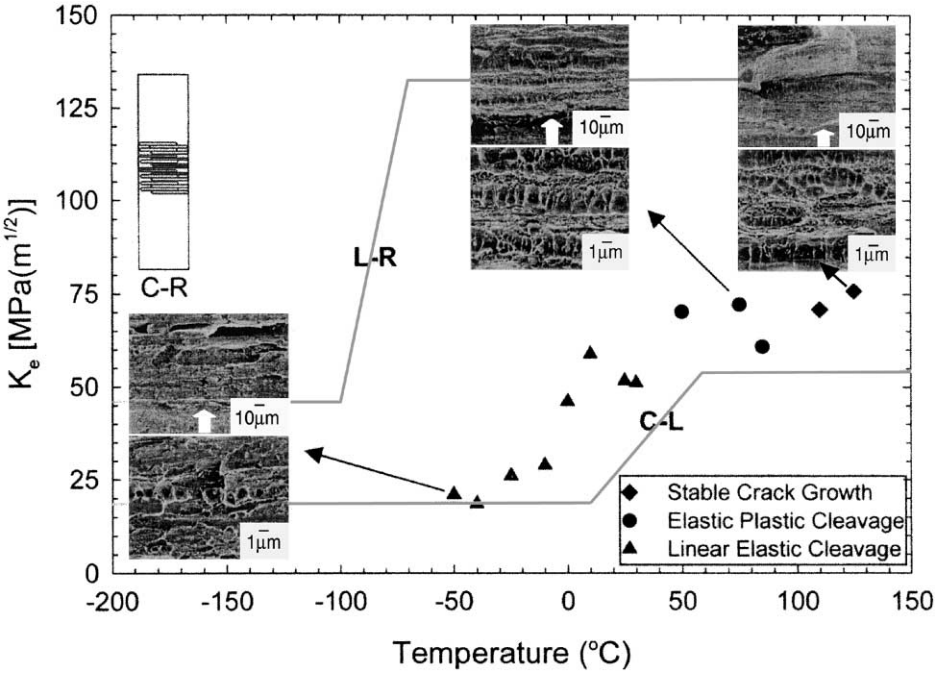

Fig. 3. K_e vs. test temperature and corresponding micrographs for the C–R orientation.

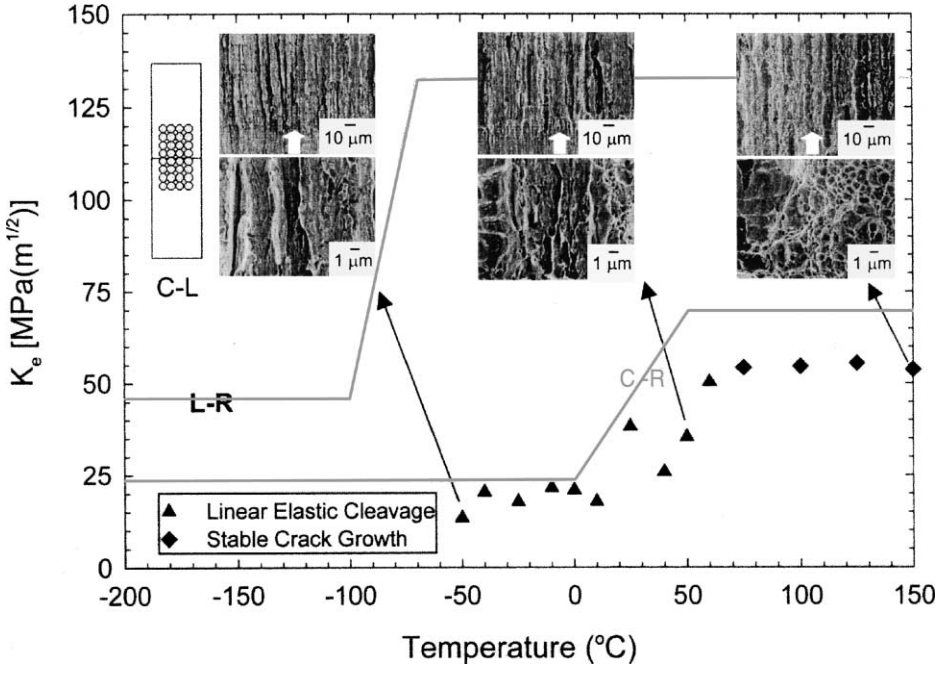

Fig. 4. K_e vs. test temperature and corresponding micrographs for the C–L orientation.

Fig. 4 shows results for the C–L orientation, which has the lowest toughness. While the toughness is approximately linear elastic up to up to 75 °C, with toughness ranging from 20 to 50 MPa $\sqrt{}$m. Above 100 °C it appears that stable crack tearing occurs close to or even before general yield at an even lower K_m (K_{Ic}) of

only 60 MPa $\sqrt{m}$. The micrographs, for the C–L orientation show a very flat fracture surface with only limited indications of ductile fracture, split inclusions and a minimal difference between the pre-crack and predominantly cleavage surface.

3.2. Tensile properties

Figs. 5 and 6 summarize the results from tensile testing. Fig. 5(a) shows the yield stress (σ_y) as a function of test temperature and Fig. 5(b) of the corresponding total engineering plastic strain at fracture. Fig. 6 provides cross sectional views and isometric diagrams indicating the macroscopic fracture surface orientation with respect to the tensile axis. As is evident from the curves and micrographs, there is also strong anisotropy in the tensile deformation and fracture properties and processes.

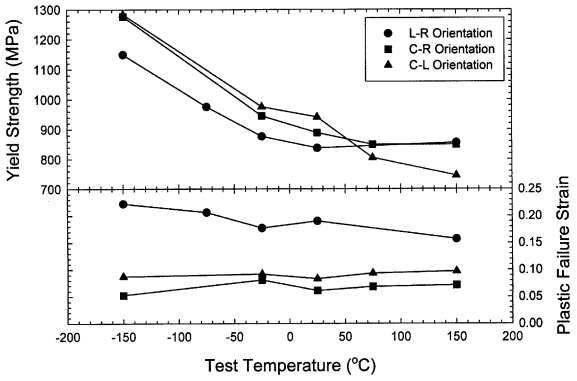

Fig. 5. Yield strength and plastic failure strain vs. test temperature for all orientations.

At low temperatures σ_y is similar and slightly higher for both C–L and C–R orientations, in which the stingers and elongated grains are oriented roughly perpendicular to the tensile axis, compared to the L–R orientation, where the elongated microstructure is parallel to the tensile axis. At the highest temperature the σ_y are similar for the L–R and C–R orientations and slightly lower in the C–L orientation. The reasons for these temperature dependent σ_y differences are not yet fully understood, since for example, the L–R orientation might be expected to benefit from some level of 'fiber reinforcement'. We speculate that the alumina stringers may be highly damaged and broken or cracked; hence the ends of broken axial segments act like pre-existing voids. In contrast, however, the plastic failure strain is only slightly dependent on temperature in the L–R orientation, but is substantially higher in this case than for the C–R and C–R orientations. These differences can be understood based on the deformation-fracture patterns illustrated in Fig. 6. Failure in the C–L and C–R orientations is dominated by shear bands oriented in the thickness (C–R) or width directions (C–L). Note that the fracture surfaces are flatter at the lowest temperatures in both these cases. In contrast, failure in the L–R orientation indicates a more classical microvoid-coalescence shear lip process at all temperatures.

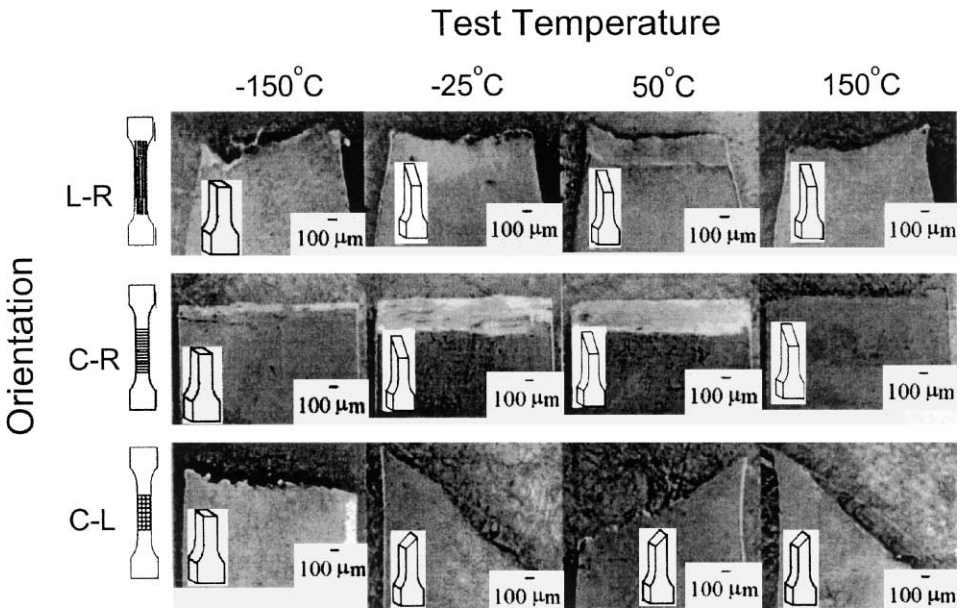

Fig. 6. Tensile fracture micrographs for all orientations.

4. Discussion

The fracture toughness and tensile data trends reflect the high degree of microstructural anisotropy and the deleterious effects of the alumina stringers on both cleavage and microvoid coalescence micro-modes of fracture. The highest toughness and ductility occurs when the crack grows across the short dimension of the elongated grains and orthogonal to the alumina stringers (L–R). Toughness and ductility are much lower in both the orientations where the stringers lie in the fracture planes (C–R and C–L). Indeed, the large anisotropy in properties probably plays a role in the relatively high toughness in the L–R orientation, since this enhances out-of-plane mixed mode fracture paths. The crack path effects appear to offset the expected direct deleterious consequence of the stringers in this orientation. At lower temperatures the in-plane stringers act as efficient cleavage microcrack nucleation sites, and they themselves provide an extended low toughness brittle fracture path, particularly in the C–L orientation, which manifests the flattest crack path. At slightly higher temperatures the stringers act as effective microvoid nucleation sites. Indeed the ductile initiation and tearing resistance is so low in these cases, that continuous cleavage is suppressed even at very low levels of toughness.

The most important tentative conclusion is that the alumina stringers, rather than the anisotropic grain structure per se, are the proximate and dominant cause of low toughness. The evidence supporting this conclusion is somewhat circumstantial (e.g. fractographic observations coupled with the mechanical property trends), since we do not have data for alloys with elongated grains without stringers to make direct comparisons. Such experiments are planned and will be reported in the future. Further, while it is beyond the scope of this paper, detailed micromechanical finite element based modeling of the deformation and fracture processes will be carried out to better assess the role of the stringers and anisotropic grain structures.

Clearly, however, the generally low, and highly orientation-dependent toughness of this MA957 product does not provide acceptable levels of performance for fusion applications. The results in the C–R and C–L orientation are important primarily for fundamental reasons. A route to high toughness and strength NFAs is shown by the results for the L–R orientation, probing conditions of crack growth in the direction of small grain dimensions and minimizing the role of inclusions as the trigger particles for cleavage and microvoid nucleation sites. These results indicate that elimination of the brittle alumina stringers and possibly a reduction in the anisotropic grain morphology will likely provide NFAs with good toughness, very high strength and good corrosion resistance.

Acknowledgements

This work was supported in part by the Office of Fusion Energy, DOE, Grant no. DE-FG03-87ER-52143. The authors would like to thank Dr D. Gelles for the providing the MA957 material and technical information and a number of interesting technical discussions.

References

[1] T. Okuda, M. Fujiwara, J. Mater. Sci. Lett. 14 (1995) 1600.
[2] J.J. Fischer, US Patent 4,075,010, Dispersion Strengthened Ferritic Alloy for use in Liquid Metal Fast Breeder Reactors, February 21, 1978.
[3] M.L. Hamilton et al., Fabrication Technological Development of the Oxide Dispersion Strengthened Alloy MA957 for Fast Reactor Applications, PNNL-13168, PNL, Richland, WA, 2000.
[4] INCO Limited, 145 King Street West, Toronto, Ontario M5H 4B7, Canada.
[5] ASTM E399-90, in: Annual Book of ASTM Standards, American Society for Testing and Materials, 1996, p. 407.
[6] ASTM E1921-97, in: Annual Book of ASTM Standards, American Society for Testing and Materials, 1998, p. 1068.
[7] ASTM E8-96, in: Annual Book of ASTM Standards, American Society for Testing and Materials, 1996, p. 55.